Separation and Purification Technology 67 (2009) 312–318

Contents lists available at ScienceDirect

Separation and Purification Technology

journal homepage: www.elsevier.com/locate/seppur

Adsorption and visible-light-derived photocatalytic kinetics of organic dye on Co-doped titania nanotubes prepared by hydrothermal synthesis

Chien-Te Hsieh*, Wen-Syuan Fan, Wei-Yu Chen, Jia-Yi Lin

Department of Chemical Engineering and Materials Science, Yuan Ze Fuel Cell Center, Yuan Ze University, Taoyuan 320, Taiwan

ARTICLE INFO

Article history:
Received 23 November 2007
Received in revised form 19 March 2009
Accepted 20 March 2009

Keywords:
Titania nanotubes
Hydrothermal treatment
Cobalt doping
Visible-light photocatalysis, Adsorption

ABSTRACT

A hydrothermal treatment combined with metal doping was employed to prepare highly porous Co-doped TiO_2 nanotubes (TNTs) for enhancement of adsorption and visible-light-driven photocatalysis capabilities of basic violet 10 (BV10) from liquid phase. The specific surface area of prepared TNTs can reach the maximal value of ~379 m^2/g. These tubes are hollow scrolls with a typical outer diameter of about 10–15 nm, inner diameter 5–10 nm and length of several micrometers. The anatase-type of TNTs has an average Co-dopant concentration of 5×10^{20} ions/cm^3, determined by an electron dispersive X-ray spectrometer. The adsorptive surface coverage on TNTs was found to be *ca.* 7.61–7.63%, showing a low affinity between BV10 molecules and TNTs. A pseudo-second-order reaction model was used to fit with the experimental data of adsorption and photocatalystic kinetic curves. The adsorption rate constant has one order higher than the photocatalytic rate constant, reflecting that the photocatalysis of the basic dye is the rate-determining step during the adsorption/photocatalysis process. These novel Co-doped TNTs are believed to be a promising candidate in a variety of photocatalysis applications because of the combination effect of a high porosity with a photocatalysis under visible illumination.

1. Introduction

Recently, tubular type of titanium dioxide (TiO_2) has attracted considerable attention because of a variety of technological and scientific applications, involving organic light-emitting diodes, photocatalysts, gas sensors, and dye-sensitized solar cells [1–6]. Several approaches to prepare TiO_2 nanotubes (TNTs) are believed to positively raise the applicability of the titania nanotubes. Among these approaches, the hydrothermal synthesis of nanotubes is an emerging method as a result of its convenience and cheapness. Generally, these TNT samples show not only high aspect ratio but also vast pore structure owing to their unique tubular-type nanostructure. Therefore, the titania-based nanotube becomes one of the promising candidates for use in photocatalytic (e.g., de-NO_x catalyst) [5] and photoelectrochemical (e.g., electrodes of dye-sensitized solar cell) systems [7]. To make it more commercial, some important characteristics of TNTs, such as adsorption and photocatalysis, still require a better understanding.

Doping metal or nonmetal has been extensively applied to improve the properties of oxide nanoparticles in catalysis and gas sensing [8,9]. Accordingly, doping transition metals into anatase-type titania crystallites leads to tune the optical band gap, thus shifting UV absorption to visible-light absorption. Pervious studies have reported doping of TiO_2 with various species such as a number of metal ions such as Pt, V, Ni, Mn, Cr and Fe [10–13], or nonmetals like N atoms [14–17]. They have been demonstrated to improve the photocatalytic reactivity toward organic molecules under visible-light illumination. Very recently, we have reported a hydrothermal route for preparation of titania nanoparticles with Fe, Co, and Ni dopants, showing a photocatalytic capability of organic dye under visible illumination [9]. However, to our knowledge, little work has been reported on probing the photocatalysis of dye on the metal-doped TNT nanostructures.

In this work, our interest focuses on adsorption and photocatalytic abilities of organic dye on metal-doped TNTs in aqueous solution. We aim to synthesize a novel titania nanostructure that behaves not only as high porosity but also as visible-light-derived photocatalysis. A hydrothermal route combined with metal doping was carried out to suit the above goals. Doping of cobalt was used to narrow the band gap of TNTs that can effectively facilitate visible-light photocatalysis capability of organic compounds. To examine the photocatalysis effect, the photocatalysis of a basic dye on Co-doped TNTs was investigated. A well-known dye, basic violet 10 (BV10), has been used in a variety of applications such as dermatological agent, veterinary medicine, and so on. The basic dye was employed here to examine the adsorption/photocatalysis hybrid capability of the TNT samples. We believe that adsorption or photodegradation of the dye from wastewater is an important

* Corresponding author. Tel.: +886 3 4638800x2577; fax: +886 3 4559373.
E-mail address: cthsieh@saturn.yzu.edu.tw (C.-T. Hsieh).

1383-5866/$ – see front matter © 2009 Elsevier B.V. All rights reserved.
doi:10.1016/j.seppur.2009.03.041

unit operation because this dye is a mutagen and mitotic poison [18,19]. Here, we discover two pathways for removal of the dye on highly porous TNTs: adsorption and visible-light-derived photocatalysis. Thus, this effort to examine the adsorption and photocatalysis kinetics (e.g., rate constant) and equilibrium parameters (e.g., adsorption and photocatalytic capacities) is devoted. In addition, the influence of porous characteristics on these parameters is also discussed.

2. Experimental

2.1. Preparation of Co-doped TNTs

The hydrothermal method combined with Co-doping was employed here for the synthesis of Co-doped TNTs. Briefly, commercial TiO_2 nanoparticles (2 g) were mixed in an aqueous solution, containing 10 M NaOH + 0.01 M $Co(NO_3)_2$, and charged into a Teflon-lined autoclave. The autoclave was then oven-heated at 135 °C for 24 h. The precipitate was filtered and the pH value of the slurry was adjusted with a diluted 0.1 M HNO_3. To obtain anatase-type titania, the pH value of the slurry was adjusted to 1.6 by HNO_3 washing [20]. The final products were obtained by filtration with subsequent drying at 110 °C overnight. For comparison, different TNT samples were prepared to examine the effect of porous characteristics on the photocatalytic capability. Three types of TNT samples with different porosities were obtained through various calcination temperatures, ranging from 300 °C to 400 °C.

2.2. Characterization of Co-doped TNTs

A UV spectrometer (Varian Cary100) was applied to analyze the reflectance spectra of TNT samples, ranging from 200 nm to 800 nm in wavelength. The phase identification of TiO_2 nanotubes was characterized by XRD with Cu Kα radiation using an automated X-ray diffractometer (Philip PW 1700). High-resolution transmission electron microscopy (HR-TEM, JEOL JEM-6500F) was

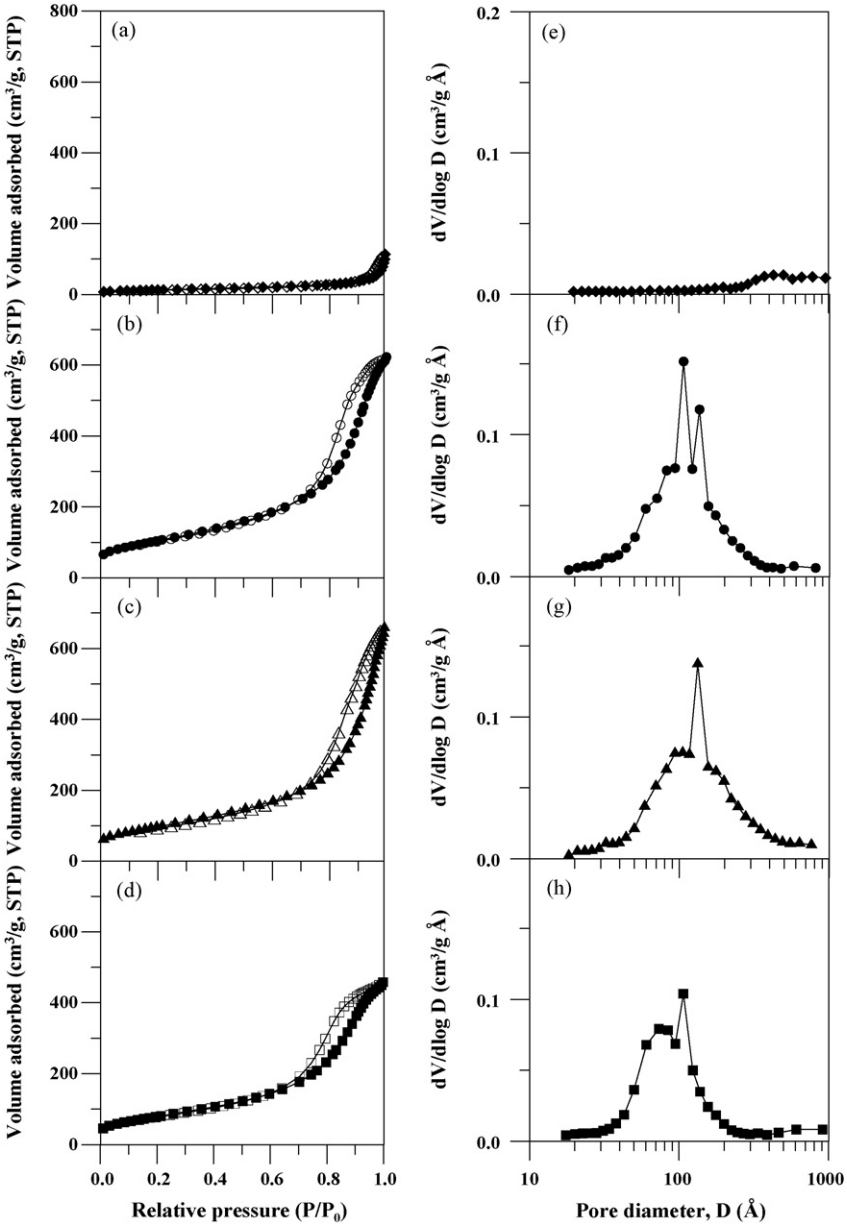

Fig. 1. Adsorption (solid symbol)/desorption (empty symbol) isotherms of N_2 onto (a) TiO_2 nanoparticles (P25), (b) TNT-1, (c) TNT-2, and (d) TNT-3 at −196 °C. Pore size distributions of (e) TiO_2 nanoparticles (P25) and (f) TNT-1, (g) TNT-2, and (h) TNT-3, determined from BJH method.

used for morphological observations of the Co-doped TNTs. Specific surface areas and pore volumes of the derived nanotubes were determined by gas adsorption. An automated adsorption apparatus (Micromeritics, ASAP 2000) was employed for these measurements. Adsorption of N_2, as a probe gas, was performed at −196 °C. Nitrogen surface areas and micropore volumes of the samples were determined from Brunauer–Emmett–Teller (BET) and Dubinin–Radushkevich (DR) equations, respectively. The amount of N_2 adsorbed at relative pressures near unity (P/P_0 = 0.98 in this work) has been employed to determine the total pore volume, which corresponds to the sum of the micropore and mesopore volumes. The peak pore diameter of nanotubes can be estimated according to pore size distribution, determined from Barret–Joyner–Halenda (BJH) method.

2.3. Adsorption and photocatalysis of BV10 on Co-doped TNTs

Analytical-grade basic dye, BV10 (molecular formula: $C_{28}H_{31}ClN_2O_3$; molecular weight: 478.5; supplier: Sigma Chemical Co.) was served as the target organic pollutant for adsorption and photocatalysis experiments. To clarify the effects of adsorption and photocatalysis, adsorption experiments of BV10 in complete darkness were performed before photocatalysis. We placed a certain amount of TNTs and 100 cm^3 of the prepared aqueous solution into a glass-stoppered flask. The flask was then put in a constant-temperature shaker bath with a revolution speed of 100 rpm. The adsorption temperature and period employed here were 40 °C and 5 h, respectively. After dark adsorption, the photodegradation of BV10 on TNTs was carried out to examine the photocatalytic reactivity under visible illumination. The photocatalytic decomposition of BV10 solutions was characterized by a UV–visible spectrometer (Shimadzu UV-2550). Based on the Beer–Lambert law [21], the dye concentration is linearly proportional to the absorbance of measured spectrum within the concentration range around 30 mg/L. The BV10-adsorbed titania slurries were also illuminated at 40 °C, employing a fluorescent lamp. To ensure no UV light illumination, the irradiation from the fluorescent lamp was filtered through a UV cut filter (Newport FSQ-GG 400), which allows the visible light > 400 nm to pass through the filter. The incident intensity of illumination from the visible light was set at 40 lx.

3. Results and discussion

Fig. 1(a)–(d) shows adsorption and desorption isotherms for a series of Co-doped TNT samples at −196 °C. The as-synthesized nanotube samples were designated as TNT-1, TNT-2, TNT-3, respectively, according to the order of N_2 adsorption capacity. The isotherm of P25 is also used to compare with TNT samples. Obviously, adsorption capacities of TNTs are much higher than that of P25. These isotherms of TNTs are found to have a hysteresis behavior within high pressure of 0.6–0.98, reflecting that the products are mainly mesoporous. The pore structures of TNT samples determined according to the adsorption data are also collected in Table 1. The specific surface areas in a range of 289–379 m^2/g are much higher than the starting material P25, which has a surface area of *ca.* 45.8 m^2/g. As expected, TNTs have a great mesopore fraction, ranging from 83% to 88%. Thus, the BJH method was employed to analyze the pore size distributions and the results are depicted in Fig. 1(e)–(h). The distributions are relatively narrow, ranging between 8 nm and 15 nm. We infer that both tips of nanotubes are opened and their inner cavities are accessible to N_2 gas molecules. Therefore, the enhancement of pore volume can be mainly contributed by the tubular-type TNTs. This type of mesoporous titania is credited to show an excellent performance in further photocatalysis and photovoltaic devices.

Table 1
Surface characteristics of P25 and Co-doped TNTs determined from N_2 physisorption at −196 °C.

Sample no.	S_{BET}[a] (m^2/g)	V_t[b] (cm^3/g)	Pore size distribution	
			V_{micro}[c] (%)	V_{meso}[d] (%)
P25	45.8	0.121	0.016 (16)	0.102 (84)
TNT-1	379	0.934	0.117 (13)	0.816 (87)
TNT-2	350	0.975	0.118 (12)	0.857 (88)
TNT-3	289	0.685	0.118 (17)	0.567 (83)

[a] S_{BET}: specific surface area computed using BET equation.
[b] V_t: total pore volume estimated at a relative pressure of 0.98.
[c] V_{micro}: micropore volume determined from DR equation.
[d] V_{meso}: mesopore volume determined from the subtraction of micropore volume from total pore volume.

Fig. 2(a) and (b) represents HR-TEM images of Co-doped TNTs with low- and high-magnification, respectively. The as-grown Co-TiO_2 nanotubes are generally homogeneous, showing narrow size distribution. The outer tube size, judged from the HR-TEM image, ranges between 10 nm and 15 nm, in agreement with the results evaluated from the BJH method. Both their ends are opened, which is extremely critical for their adsorption and photocatalysis capability. As observed from Fig. 2(b), the nanotubes are scrolls (unlike carbon nanotubes), showing unequal number of walls on both tube sides. The typical nanotube axis is mostly along the [1 0 0] direction of the anatase crystalline structure, and the interspacing of the tube walls is around 0.78 nm. Indeed, this transformation of TiO_2 precursor to anatase-type titania nanotube has been well examined and reported elsewhere [1,20]. This result is consistent with the pervious studies, confirming the anatase-type TNTs [22].

Electron dispersive X-ray spectrometer (EDS) was used to confirm the composition of TNT samples, as shown in Fig. 3. The EDS analysis has showed the presence of Co in TiO_2 crystallites, and the average dopant concentration of TNTs is found to be 5×10^{20} ions/cm^3. Fig. 4 compares the typical XRD patterns of TNTs and P25. It is known that the precursor P25 has *ca.* 70% anatase and *ca.* 30% rutile phases. In the case of TNTs, the XRD patterns that the representative peaks are anatase [1 0 1], [0 0 4], [2 0 0], [1 0 5], and [2 0 4] diffractions at scattering angles (2θ) of 25.3°, 36.6°, 48.0°,

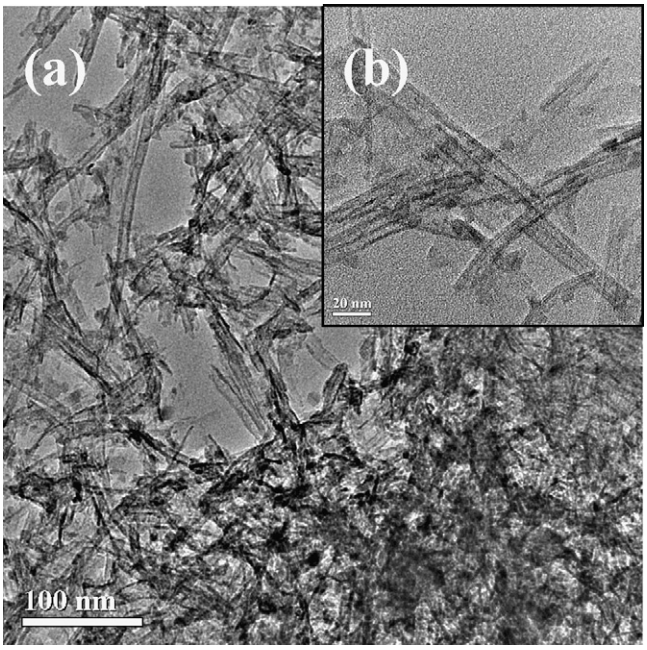

Fig. 2. Typical HR-TEM image of as-prepared Co-doped TNTs with (a) low and (b) high magnifications.

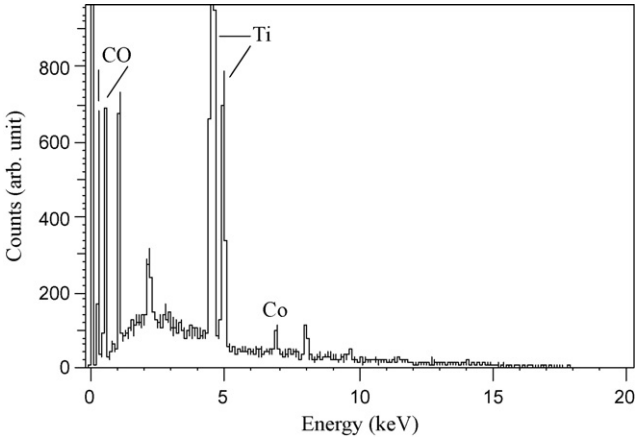

Fig. 3. EDS pattern of as-prepared Co-doped TNTs (sample: TNT-2).

54.5°, and 62.6°, respectively. Apparently, the rutile of P25 has been transformed to anatase-type. The anatase phase with a longer *c*-axis has been reported to be the preferred phase in TiO_2 nanotubes [20,22]. Additionally, the peak intensity becomes vague after the formation of nanotubes. This is presumably due to the small number of crystalline layers or the small wall thickness of the tubes.

Diffuse reflection spectra of TNTs and P25 are shown in Fig. 5. Generally, anatase-type TiO_2 crystalline has a strong absorption edge below *ca.* 380 nm [10]. In comparison, the absorption edge of Co-doped TNTs shows a shift to visible-light region, i.e., > 400 nm in wavelength. After that, an obvious peak appears within the wavelength region 550–650 nm, which can be ascribed to the formation of impurity energy level within the band gap. This proves that the hydrothermal doping technique has modified the UV–visible absorption characteristics of titania catalysts. In Fig. 5, both the absorption edges are extrapolated to the axis of wavelength, producing two intersections: (A) and (B) at 385 nm and 590 nm, respectively. Generally, the intersection represents the optical band gap of titania samples according to the formula of band gap (optical

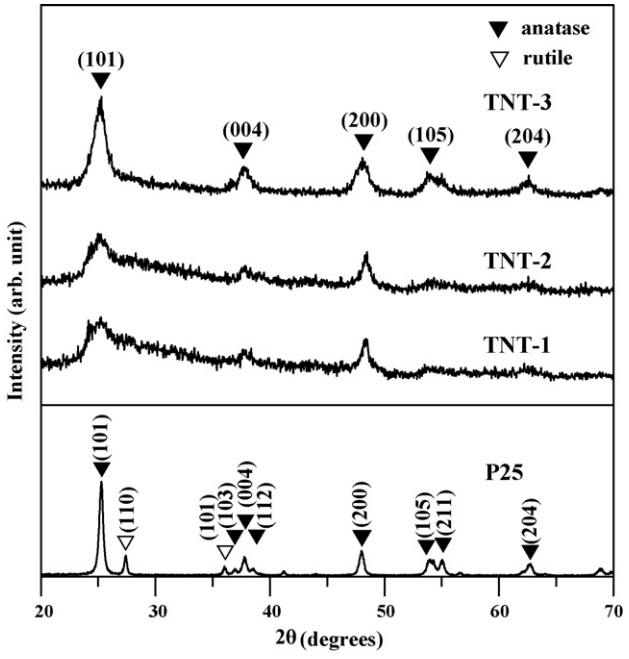

Fig. 4. XRD patterns for Co-doped TNTs prepared from the hydrothermal treatment. In the bottom of this figure, the XRD pattern of P25 shows *ca.* 70% anatase and *ca.* 30% rutile phases.

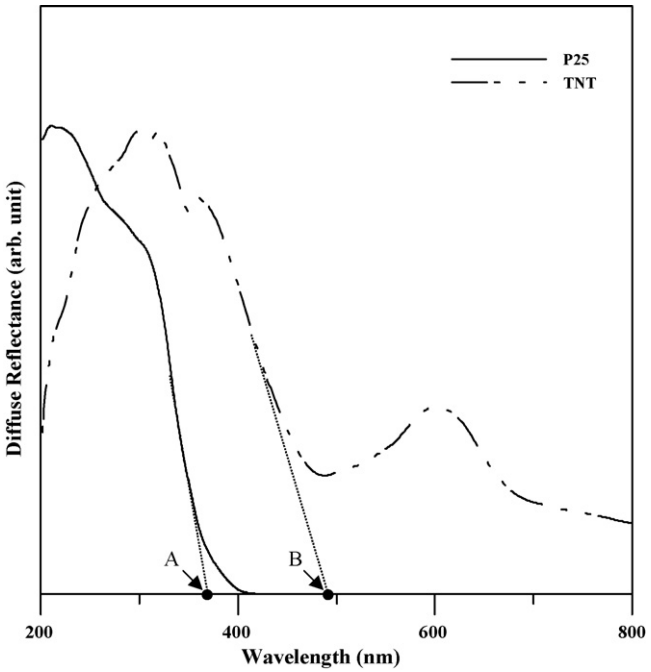

Fig. 5. Diffuse reflection spectra for TiO_2 nanoparticles (P25) and Co-doped TNTs.

band gap = 1240/wavelength). After calculations, P25 has a typical band gap of 3.20 eV, whereas the Co-doped TNT shows a significant drop of the magnitude of band gap smaller than 3.20 eV; that is, only *ca.* 2.14 eV for all Co-doped TNTs. The above results disclose one crucial finding that the Co-dopants effectively make the band gap narrower. Also, this confirms that the hydrothermal synthesis of Co-doping in TNTs leads to a pathway of "communicated electrons" between these crystals. How the Co doping in TNTs affects the visible-light photocatalysis of organic dye will be investigated in the following section.

We now turn to the main subject of this paper, that is, the adsorption and visible-light photocatalysis behaviors of the Co-doped TNT samples. The adsorption and photocatalytic kinetics as functions of time are shown in Fig. 6. To figure out both the effects, the adsorption experiment in complete darkness was carried out first, followed by the photocatalysis of BV10 under visible illumination. The adsorption equilibrium of BV10 is reached within 2 h, and the equilibrium adsorption capacities have an order as follows: TNT-1 (10.6 mg/g) > TNT-2 (9.8 mg/g) > TNT-3 (8.1 mg/g) ≫ P25 (0.35 mg/g). These total adsorption capacities of TNTs are much greater than that of P25 nanoparticles [23]. In the case of adsorption of BV10 on the Co-doped TNTs, this order is generally followed by the magnitude of specific surface area of nanotubes, indicating different numbers of active sites for the liquid-phase adsorption of dye molecules.

The adsorptive surface coverage Θ_{ads}, i.e., the fraction of BET area covered by BV10 molecules, can be estimated by assuming that the area occupied by a BV10 molecule is estimated to be 217 $Å^2$ [24]. The calculated surface coverage Θ_{ads} for TNTs ranges between 7.61% and 7.63%, showing that all Co-doped TNTs have the same number of active sites for adsorption of BV10. However, such low Θ_{ads} value (≪100%) reflects that basic dyes only partially wet titania surface (or low affinity between BV10 molecules and TNTs), indicating the presence of surface heterogeneity for BV10 adsorption. It is generally recognized that the adsorption of basic dyes on adsorbents is dominated by ion-exchange process [25]. Since TiO_2 surface favors a more hydrophilic behavior due to surface hydroxyl (—OH) groups [3], whereas the polarity of BV molecule seems to be weak, thus resulting in the weak interaction between TNTs and BV10. Another

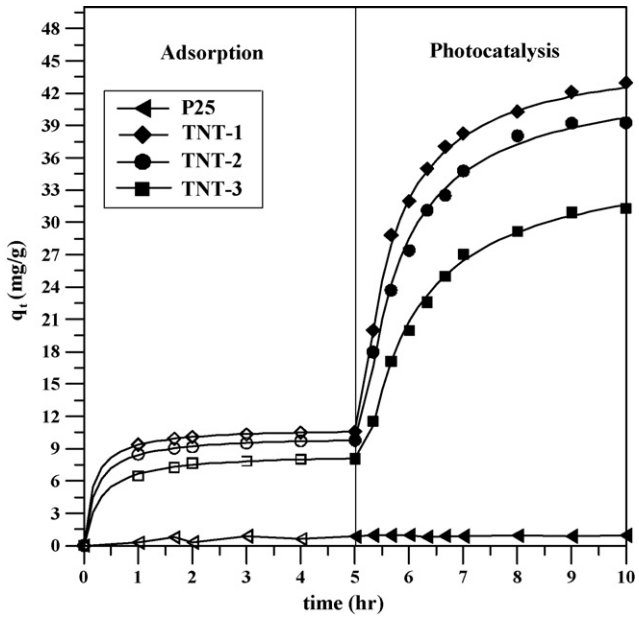

Fig. 6. Dark adsorption of BV10, followed by visible-light photocatalysis kinetic curves for TiO_2 nanoparticles (P25) and different Co-doped TNTs at 40 °C.

way to interpret the above result is probably due to the fact that the large basic dyes may screen TNT porosity. This would induce the inaccessibility for BV10 into the entrance or channel of TNTs, decreasing available N_2-BET surface area for adsorption of the basic dye.

Fig. 6 also shows visible-light photocatalytic kinetics of BV10 on Co-doped TNTs after attaining adsorption saturation. As expected, P25 does not show any photocatalytic capability under visible irradiation. On the contrary, Co-doped TNTs are found to give an excellent photodecomposition performance of BV10 in liquid phase. This demonstrates that the hydrothermal synthesis of Co-doped TNTs is an efficient approach in promoting not only adsorption but also photocatalysis ability under visible illumination. Their photocatalytic capacities after 10 h visible illumination have an order as follows: TNT-1 (43.0 mg/g) > TNT-2 (39.2 mg/g) > TNT-3 (29.5 mg/g) ≫ P25 (~0.1 mg/g). This sequence of photocatalysis is identical with adsorption capacity, which is strongly related to the porosity of TNT samples. The results disclose two important messages: (i) the photocatalysis of BV under visible illumination belongs to a surface-catalyzed reaction, and (ii) the pore structure of Co-doped TNTs may play a major factor in removing the dye form aqueous solution.

Here, we estimate the photocatalytic surface coverage, Θ_{photo}, according to the above assumptions. These calculated Θ_{photo} values are 30.87%, 30.48%, and 29.47% for TNT-1, TNT-2, and TNT-3, respectively. This little difference indicates a resembling amount of active sites over TNTs for visible-light-derived photocatalysis of BV10. It is of interest that the Θ_{ads} has a much smaller value than the Θ_{photo}, which can be attributed to two possible reasons: (i) the number of adsorptive sites cannot match that of photocatalytic sites at an equal rate constant or (ii) the equilibrium rate constant of adsorption exceeds that of visible-light photocatalysis. Generally, the photocatalytic reaction is considered as a surface-catalyzed reaction that would take place on the dye-adsorbed sites over photocatalysts. This means that the surface coverage of photocatalytic sites should be identical with that of adsorptive sites based on equal rate constants. However, this result seems to violate the above assumption in our case. Thus, we infer that reason (ii) suits to the adsorption/visible-light photocatalysis hybrid behavior of BV10 on Co-doped TNTs. To prove this, the adsorption and photocatalysis kinetic parameters will be investigated in further section.

It is known that Langmuir–Hsinshelwood kinetic model presents a well description on the dependency of photocatalytic reaction rates of organic compounds [26–28]. However, this model cannot agree with the adsorption/photocatalytic kinetics of BV10 on TNTs based on the above deduction. Accordingly, a simple reaction rate expression is performed with the aid of pseudo-second-order equation [25,29] as follows:

$$\frac{dq_t}{dt} = k(q_e - q_t)^2 \quad (1)$$

where q_e and q_t are the amount of BV10 adsorbed or visible-light photocatalyzed per unit mass of TNT at steady state and any time t, respectively, and k_{ads} is the rate constant for adsorption (k_{ads}) and photocatalysis (k_{photo}) of BV10. This adsorption rate expression can be definitely integrated by applying the two initial conditions $q_t = 0$ at $t = 0$ and $q_t = q_t$ at $t = t$.

$$\frac{t}{q_t} = \frac{1}{k_{ads}q_e^2} + \frac{t}{q_e} \quad (2)$$

A linearity plot of t/q_t versus t would determine q_e and k_{ads} from the slope and intercept, respectively. The calculated values, together with the correlation factor (r^2), are given in Table 2. The r^2 value, approximately close to unity, indicates an excellent fitting result for the adsorption of BV10 on TNTs using the pseudo-second-order kinetic model. As shown in Table 2, all q_e values are nearly identical with the equilibrium adsorption capacities determined from Fig. 6. These rate constants, k_{ads}, are found to have an increasing function of BET specific surface area, ranging between 6.6×10^{-3} g/min mg and 8.9×10^{-3} g/min mg. Basically, Eq. (1) is an apparent reaction formula; that is, the rate constant is possibly governed by diffusion and adsorption in the BV10 adsorption step. Since all TNTs show the similar pore size distribution (Fig. 1) and tubular size (Fig. 2), we infer that pore diffusion resistance has the same basis during the adsorption process. Thus, the increase in the adsorption rate constant can be ascribed to the fact that the vaster porosity of TNTs provides more active sites, allowing BV10 accessibility into nanotubes.

Similarly, Eqs. (1) and (2) are employed to estimate the kinetic parameters of visible-light photocatalysis once again. It is noticed that the initial conditions should be modified since each TNT has its own adsorption capacity at steady state. The apparent rate constant for visible-light photocatalysis (k_{photo}) and photocatalytic capacity (q'_e) can be determined from the intercept and slope of linearity plot of t/q_t versus t, respectively. The two parameters, together with correlation factor (r^2), of pseudo-second-order reaction are also collected and listed in Table 2. The r^2 values (>0.995) demonstrate that

Table 2
Adsorption and visible-light photocatalytic parameters on Co-doped TNTs determined from the pseudo-second-order reaction kinetic model.

Sample no.	Dark adsorption			Visible-light-derived photocatalysis		
	q_e (mg/g)	k_{ads} (g/min mg)	r^2	q'_e (mg/g)	k_{photo} (g/min mg)	r^2
TNT-1	10.9	0.0089	0.997	46.3	0.00082	0.999
TNT-2	10.2	0.0076	0.998	40.0	0.00072	0.997
TNT-3	8.6	0.0066	0.995	30.3	0.00060	0.998

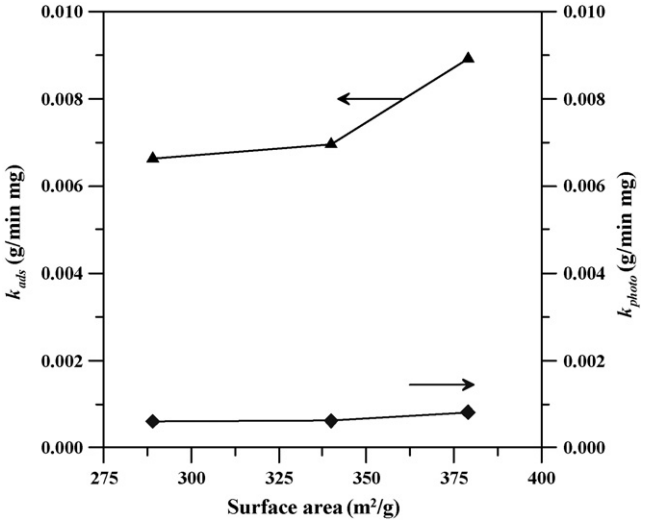

Fig. 7. Variations of the rate constants for adsorption and visible-light photcatalysis of BV10, determined from the pseudo-second-order reaction kinetic model, with the BET specific surface area of Co-doped TNTs.

the linear fits are fairly good for photocatalytic kinetic behavior of BV10. These kinetic parameters in Table 2 are used to predict the adsorption and photocatalysis kinetic curves of Co-doped TNTs, and the prediction curves are presented in Fig. 6 to compare with the experimental data. Fig. 6 clearly shows that Eq. (1) provides equally good fits for all the TNT samples over the entire reaction period.

From the data in Table 2, the visible-light photocatalytic capacity, q'_e, is expected to have an increasing trend of the specific surface area of TNTs. Again, this proves that the specific surface area significantly promotes the number of active sites for photocatalysis under visible illumination. As for the value of k_{photo}, it also depends on the specific surface area of TNTs, showing an increase in k_{photo} value with the porosity. To compare with the k_{ads} value, the two rate constants as function of the specific surface area are illustrated in Fig. 7. This figure shows that both the rate constants tend to gradually increase with surface area. Reasonably, this positive effect informs that more active sites over photocatalysts facilitate the adsorption and photocatalytic rates. Additionally, we note that the k_{ads} value has one order higher than the k_{photo} value. This finding can support our pervious argument that the equilibrium rate constant of adsorption exceeds that of visible-light photocatalysis, thus resulting in adsorptive surface coverage smaller than photocatalytic coverage. Based on the result, we infer that the photocatalysis of BV10 under visible illumination becomes the rate-determining step during the adsorption/photocatalysis hybrid process.

As mentioned above, it is generally admitted that the adsorption of basic dye on adsorbents is a simple physisorption [25,29,30]. However, visible-light photocatalysis is a serial of complicated reactions, consisting of photoinduction, electron (e^-)/hole (h^+) pair generation, radical formation, and BV10 degradation. Briefly, the formation of (e^-)/hole (h^+) pairs on Co-doped TNTs requires a photoexcited energy of 2.14 eV, which is about seven times higher than the physisorption of BV10 on titanate nanotubes (~0.295 eV) [31]. This induces that the visible photocatalysis of BV10 would take a very long period in comparison with the physisorption; that is, $k_{ads} \gg k_{photo}$, as shown in Fig. 7. After the adsorption of BV10 takes place on adsorptive site rapidly, the BV10-adsorbed site is slowly photocatalyzed under visible illumination, thus decomposing the dye into one ionic compound. After that, next BV10 molecule immediately occupies the site, and the photocatalysis then repeats to degrade next +BV10 molecule. Owing to the well-developed tubular nanostructure, dye diffusion and adsorption resistance seem to be negligible. When the photocatalysis period prolongs, the number of photoactive species is enough to photodecompose the basic dyes, thus leading to higher visible-light photocatalytic activity. We believe that Co-doped nanotubes show not only a fairly good adsorption capacity in liquid phase but also a dye-photocatalysis capability under visible illumination.

4. Conclusions

(1) We have successfully developed a hydrothermal route for the preparation of Co-doped TNTs that markedly enhance the adsorption and visible photocatalytic capabilities of basic dye in aqueous solution.
(2) The prepared TNTs exhibit high specific surface areas of *ca.* 289–379 m^2/g and total pore volumes of 0.685–0.934 cm^3/g. HR-TEM observation showed that these tubes are hollow scrolls with a typical outer diameter of about 10–15 nm, inner diameter 5–10 nm and length of several micrometers.
(3) The crystalline structure of TNTs showed anatase-type crystallite, and the dopant concentrations of cobalt had an average value of 5×10^{20} ions/cm^3, determined from XRD and EDS analysis, respectively. In UV absorption spectra, the absorption edge of Co-doped TNTs shows a shift to visible-light region, followed by an obvious absorption peak at 550–650 nm. This transformation can be ascribed to the formation of impurity energy level within the band gap, improving the visible-light photocatalysis of basic dye.
(4) Adsorption and visible-light photocatalysis capacities are increasing functions of the BET-specific surface area, showing that (i) the photocatalysis of BV under visible illumination belongs to a surface-catalyzed reaction, and (ii) the pore structure of Co-doped TNTs may play a major factor in removing the dye form aqueous solution.
(5) The adsorptive surface coverage (Θ_{ads}) on TNTs was found to be *ca.* 7.61–7.63%, showing the low affinity between BV10 molecules and TNTs. Based on the surface-catalyzed reaction, the photocatalytic surface coverage, Θ_{photo}, ranges between 29.47% and 30.87%, which is much higher than Θ_{ads}.
(6) A pseudo-second-order reaction expression was found to have an excellent fitting with the experimental data of adsorption and photocatalytic kinetic curves. The k_{ads} value has one order higher than the k_{photo} value, reflecting that the photocatalysis of the basic dye is the rate-determining step during the adsorption/photocatalysis process.
(7) The hydrothermal synthesis of Co–TiO_2 tubes is an efficient approach in enhancing not only specific surface area but also photocatalysis capability under visible illumination. These novel Co-doped TNTs are believed to be a promising candidate in a variety of photocatalysis applications because of the combination effect of a high porosity with a photocatalysis under visible illumination.

Acknowledgments

The authors gratefully acknowledge financial support from the Ministry of Education (MOE) and the National Science Council (NSC) in Taiwan, through Project NSC 96-2221-E-155-055-MY2.

References

[1] C.C. Tsai, H. Teng, Regulation of the physical characteristics of titania nanotube aggregates synthesized from hydrothermal treatment, Chem. Mater. 16 (2004) 4352–4358.
[2] G.K. Mor, K. Shankar, M. Paulose, O.K. Varghese, C.A. Grimes, Enhanced photocleavage of water using titania nanotube arrays, Nano Lett. 5 (2005) 191–195.
[3] L. Qian, Z.S. Jin, S.Y. Yang, Z.L. Du, X.R. Xu, Bright visible photoluminescence from nanotube titania grown by soft chemical process, Chem. Mater. 17 (2005) 5334–5338.

[4] A. Ghicov, J.M. Macak, H. Tsuchiya, J. Kunze, V. Haeublein, L. Frey, P. Schmuki, Ion implantation and annealing for an efficient N-doping of TiO_2 nanotubes, Nano Lett. 6 (2006) 1080–1082.
[5] P. Umek, P. Cevc, A. Jesih, A. Gloter, C.P. Ewels, D. Arčon, Impact of structure and morphology on gas adsorption of titanate-based nanotubes and nanoribbons, Chem. Mater. 17 (2005) 5945–5950.
[6] H. Kim, R.C.Y. Auyeung, M. Ollinger, G.P. Kushto, Z.H. Kafafi, A. Piqué, Laser-sintered mesoporous TiO_2 electrodes for dye-sensitized solar cells, Appl. Phys. A 83 (2006) 73–76.
[7] S. Nakade, Y. Saito, W. Kubo, T. Kitamura, Y. Wada, S. Yanagida, Influence of TiO_2 nanoparticle size on electron diffusion and recombination in dye-sensitized TiO_2 solar cells, J. Phys. Chem. B 107 (2003) 8607–8611.
[8] D. Pan, G. Xu, J. Wan, Z. Shi, M. Han, G. Wang, Tuning the solubility of TiO_2 nanoparticles in apolar solvents by doping with Co^{2+}, Langmuir 22 (2006) 5537–5540.
[9] T.Y. Han, C.F. Wu, C.T. Hsieh, Hydrothermal synthesis and visible-light photocatalysis of metal-doped titania nanoparticles, J. Vac. Sci. Technol. B 25 (2007) 430–435.
[10] M. Anpo, Use of visible light. Second-generation titanium oxide photocatalysts prepared by the application of an advanced metal ion-implantation method, Pure Appl. Chem. 72 (2000) 1787–1792.
[11] M. Harada, T. Sasaki, Y. Ebina, M. Watanabe, Preparation and characterizations of Fe- or Ni-substituted titania nanosheets as photocatalysts, J. Photochem. Photobiol. A: Chem. 148 (2002) 273–276.
[12] M. Anpo, M. Takeuchi, The design and development of highly reactive titanium oxide photocatalysts operating under visible light irradiation, J. Catal. 216 (2003) 505–516.
[13] D. Dvoranová, V. Brezová, M. Mazúr, M.A. Malati, Investigations of metal-doped titanium dioxide photocatalysts, Appl. Catal. B: Environ. 37 (2002) 91–105.
[14] R. Asahi, T. Morikawa, T. Ohwaki, K. Aoki, Y. Taga, Visible-light photocatalysis in nitrogen-doped titanium oxides, Science 293 (2001) 269–271.
[15] D. Li, H. Haneda, Synthesis of nitrogen-containing ZnO powders by spray pyrolysis and their visible-light photocatalysis in gas-phase acetaldehyde decomposition, J. Photochem. Photobiol. A: Chem. 155 (2003) 171–178.
[16] M. Jansen, H.P. Letschert, Inorganic yellow-red pigments without toxic metals, Nature 404 (2000) 980–982.
[17] P.G. Wu, C.H. Ma, J.K. Shang, Effects of nitrogen doping on optical properties of TiO_2 thin films, Appl. Phys. A 81 (2005) 1411–1417.
[18] C. Sahoo, A.K. Gupta, A. Pal, Photocatalytic degradation of crystal violet (C.I. basic violet 3) on silver ion doped TiO_2, Dyes Pigments 66 (2005) 189–196.
[19] C.C. Wang, C.K. Lee, M.D. Lyu, L.C. Juang, Photocatalytic degradation of C.I. basic violet 10 using TiO2 catalysts supported by Y zeolite: an investigation of the effects of operational parameters, Dyes Pigment 76 (2008) 817–824.
[20] C.C. Tsai, H. Teng, Structural features of nanotubes synthesized from NaOH treatment on TiO_2 with different post-treatments, Chem. Mater. 18 (2006) 367–373.
[21] H.F. Lin, S.C. Liao, S.W. Hung, The dc thermal plasma synthesis of ZnO nanoparticles for visible-light photocatalyst, J. Photochem. Photobiol. A: Chem. 174 (2005) 82–87.
[22] B.D. Yao, Y.F. Chan, X.Y. Zhang, W.F. Zhang, Z.Y. Yang, N. Wang, Formation mechanism of TiO_2 nanotubes, Appl. Phys. Lett. 82 (2003) 281–283.
[23] M.L. Fetterolf, H.V. Patel, J.M. Jennings, Adsorption of methylene blue and acid blue 40 on titania from aqueous solution, J. Chem. Eng. Data 48 (2003) 831–835.
[24] R.C. Reid, J.M. Prausnitz, B.E. Poling, The Properties of Gases and Liquids, McGraw-Hill, Singapore, 1987.
[25] L.C. Juang, C.C. Wang, C.K. Lee, Adsorption of basic dyes onto MCM-41, Chemosphere 64 (2006) 1920–1928.
[26] J. Matos, J. Laine, J.M. Herrmann, Effect of the type of activated carbons on the photocatalytic degradation of aqueous prganic pollutants by UV-irradiated titania, J. Catal. 200 (2001) 10–20.
[27] J. Matos, J. Laine, J.M. Herrmann, Synergy effect in the photocatalytic degradation of phenol on a suspended mixture of titania and activated carbon, Appl. Catal. B: Environ. 18 (1998) 281–291.
[28] L. Zou, Y. Luo, M. Hooper, E. Hu, Removal of VOCs by photocatalysis process using adsorption enhanced TiO_2–SiO_2 catalyst, Chem. Eng. Process. 45 (2006) 959–964.
[29] C.K. Lee, S.S. Liu, L.C. Juang, C.C. Wang, Application of MCM-41 for dyes removal from wastewater, J. Hazard. Mater. 147 (2007) 997–1005.
[30] Y.R. Lin, H. Teng, Mesoporous carbons from waste tire char and their application in wastewater discoloration, Micropor. Mesopor. Mater. 54 (2002) 167–174.
[31] C.K. Lee, K.S. Lin, C.F. Wu, M.D. Lyu, C.C. Lo, Effects of synthesis temperature on the microstructures and basic dyes adsorption of titanate nanotubes, J. Hazard. Mater. 150 (2008) 494–503.